

Analysis of the Nitric Oxide-sensing Non-heme Iron Center in the NorR Regulatory Protein*

Received for publication, July 17, 2007, and in revised form, November 14, 2007. Published, JBC Papers in Press, November 14, 2007, DOI 10.1074/jbc.M705850200

Nicholas P. Tucker^{†1}, Benoît D'Autréaux^{‡1,2}, Faridoon K. Yousafzai[‡], Shirley A. Fairhurst[‡], Stephen Spiro[§], and Ray Dixon^{‡3}

From the [†]Department of Molecular Microbiology, John Innes Centre, Colney, Norwich Research Park, Norwich NR4 7UH, United Kingdom and the [§]Department of Molecular and Cell Biology, University of Texas at Dallas, Richardson, Texas 75083-0688

The NorR regulatory protein senses nitric oxide (NO) to activate genes required for NO detoxification under anaerobic and microaerobic conditions in *Escherichia coli*. NorR belongs to the σ^{54} -dependent family of transcriptional activators and contains an N-terminal regulatory GAF (cGMP phosphodiesterase, adenylate cyclase, FhlA) domain that controls the ATPase activity of the central AAA+ domain to regulate productive interactions with σ^{54} . Binding of NO to a non-heme iron center in the GAF domain results in the formation of a mononitrosyl-iron complex and releases intramolecular repression of the AAA+ domain to enable activation of transcription. In this study, we have further characterized NorR spectroscopically and substituted conserved residues in the GAF domain. This analysis, in combination with structural modeling of the GAF domain, has identified five candidate ligands to the non-heme iron and suggests a model in which the metal ion is coordinated in a pseudo-octahedral environment by three aspartate residues, an arginine, and a cysteine.

Gas-sensing proteins play central roles in the regulation of important biological processes. Protein sensors that respond directly to nitric oxide (NO),⁴ a free radical gas that is potentially toxic to biological systems, regulate a diverse range of cellular events. In higher eukaryotes, the major response to NO involves interaction of the NO radical with the heme moiety of soluble guanylate cyclase (1). Although heme-containing proteins may act as NO sensors in bacteria (2–5), the majority of the prokaryotic NO-sensing regulatory proteins characterized to date contain either iron-sulfur clusters (6, 7) or non-heme iron centers that interact with NO to form nitrosyl-iron complexes (8, 9).

A major function of NO-sensing pathways in enteric bacteria is to regulate the expression of genes required for NO detoxification and hence protect the organism against the NO stress

inflicted either exogenously by host phagocytic cells, or endogenously by anaerobic respiration, when nitrate or nitrite are used as terminal electron acceptors. In *Escherichia coli* only two regulatory proteins, NsrR and NorR, appear to exclusively sense NO (10). NsrR is a recently identified transcriptional repressor that probably contains an iron-sulfur cluster and regulates the expression of several genes in response to NO (11–14). One of the genes regulated by NsrR in *E. coli* is *hmp*, which encodes a flavohemoglobin with oxygen-dependent denitrosylase activity that detoxifies NO under aerobic conditions (15–18). NorR is a σ^{54} -dependent transcriptional activator that activates transcription of the *norVW* operon in *E. coli* in response to NO (19–21). The NorV flavorubredoxin and associated NorW flavoprotein exhibit NADH-dependent NO reductase activity, considered to be responsible for the detoxification of NO under both anaerobic and microaerobic conditions (22, 23).

The NorR transcriptional activator has a modular domain architecture characteristic of the prokaryotic family of σ^{54} -dependent enhancer binding proteins (24). NorR contains three domains with the following predicted functions: an N-terminal regulatory GAF domain (25, 26), a central catalytic AAA+ domain required for the interaction with σ^{54} and the coupling of ATP hydrolysis to promoter DNA melting by RNA polymerase (27), and a C-terminal domain with a helix-turn-helix motif required for interaction with specific DNA enhancer sites (28, 29). Truncated derivatives of NorR lacking the N-terminal GAF domain are competent to activate transcription in the absence of a source of NO (19, 30), suggesting firstly, that the GAF domain is responsible for NO sensing and secondly, that in the absence of the NO signal, the GAF domain controls the activity of the other domains of NorR by intramolecular repression (31). We have recently demonstrated that the GAF domain of NorR contains a mononuclear non-heme iron center that reversibly binds NO forming a paramagnetic mononitrosyl-iron complex with an $S = 3/2$ ground state (9). The spectroscopic features of this high spin complex suggest that the iron atom in the mononitrosyl adduct is 5 or 6 coordinate with electronic structure $\{\text{Fe}(\text{NO})\}^7$ according to the Enemark and Feltham notation (32). Binding of NO to the ferrous ion in the GAF domain stimulates the ATPase activity of the AAA+ domain, enabling NorR to activate transcription by σ^{54} -RNA polymerase (9). In this study, we have substituted conserved residues in the GAF domain and further characterized NorR by EPR, electronic absorption, and MCD spectroscopies. This analysis has identified five candidate ligands to the non-heme iron center and additional residues that may be involved in signal transmission. Spectroscopy in combination with struc-

* This work was supported by the Biotechnology and Biological Sciences and Research Council (Grant BB/D009588/1 to R.D.) and National Science Foundation Grant MCB-0702858 (to S.S.). The costs of publication of this article were defrayed in part by the payment of page charges. This article must therefore be hereby marked "advertisement" in accordance with 18 U.S.C. Section 1734 solely to indicate this fact.

¹ Both authors contributed equally to this work.

² Current address: Laboratoire Stress Oxydant et Cancer, SBI-GeM, iBiTec-S, CEA-Saclay, Gif-sur-Yvette 91191, Cedex, France.

³ To whom correspondence should be addressed: Tel.: 44-160-3045-0747; Fax: 44-160-3450-778; E-mail: ray.dixon@bbsrc.ac.uk.

⁴ The abbreviations used are: NO, nitric oxide; GAF, cGMP phosphodiesterase, adenylate cyclase, FhlA; AAA+, ATPases associated with various cellular activities; LMCT, ligand metal charge transfer; MCD, magnetic CD; MAHMA NNOate, (Z)-1-(N-methyl-N-[6-(N-methylammoniohexyl)amino])diazene-1,2-diolate.

tural modeling suggests that the mononuclear non-heme iron in the GAF domain is 5 or 6 coordinate, with distorted octahedral symmetry.

EXPERIMENTAL PROCEDURES

Chemicals and Biochemicals—MAHMA NONOate ((Z)-1-(N-methyl-N-[6-(N-methylammoniohexyl)amino])-diazene-1-ium 1,2-diolate) was provided by Alexis chemicals. ATP, CTP, CoCl_2 , and $\text{Fe}(\text{NH}_4)_2(\text{SO}_4)_2$ were from Sigma-Aldrich. All restriction enzymes were from Roche Applied Science.

Site-directed Mutagenesis—The QuikChange II XL site-directed mutagenesis kit (Stratagene), with pNorR2 plasmid as a template (29), was used to introduce mutations into the GAF domain of NorR. The constructs were sequenced on both strands to ensure that only the desired mutation was introduced.

Assay of NorR Activity in Vivo—Transcriptional activation by NorR *in vivo* was measured by introducing wild-type and mutant plasmids into NPT1003, a *nor::cat* derivative of *E. coli* strain MC1000 with a *lacZ* reporter fusion to the *norVW* promoter inserted at the phage λ attachment site (9). Cultures were grown with shaking in 50 ml of LB medium at 37 °C until the $A_{650\text{ nm}}$ reached 0.3, at which point glucose was added to the culture to a final concentration of 1%. Cultures were then split into 8-ml Bijou bottles and were grown anaerobically overnight at 37 °C with or without potassium nitrite (4 mM). Under these conditions, NorR is activated by the NO that is generated endogenously by nitrite reduction in *E. coli* (9). Levels of expression of the *norV-lacZ* fusion were then determined by assaying β -galactosidase activity as described previously (29).

Whole Cell EPR Spectroscopy—Freshly transformed bacteria were grown anaerobically at 30 °C in 25 ml of LB medium containing 1% glucose (w/v) and 100 $\mu\text{g}/\text{ml}$ carbenicillin. Expression of NorR and GAF_{NorR} was induced at $A_{600\text{ nm}} = 0.6$ with 50 μM isopropyl 1-thio- β -D-galactopyranoside. After 3 h, MAHMA NONOate (final concentration, 200 μM) was added and incubation continued for 15 min ($t_{1/2} = 3$ min, pH = 7.5, 30 °C). The cells were harvested at 4000 rpm for 10 min, and the pellets were resuspended in 0.5 ml of 100 mM Tris-HCl (pH 7.5), 25 mM NaCl, 10% glycerol (v/v). Cell suspensions were transferred to an EPR tube and immediately frozen.

Purification of Mutants and Co^{2+} -substituted NorR—NorR mutants were purified under anaerobic conditions as described previously (9). Apo-NorR mutants were obtained after heparin and gel-exclusion chromatography. Because iron was lost during the gel-filtration step, iron-containing proteins were obtained after the heparin step. The Co^{2+} -substituted NorR was purified aerobically according to the previous procedure, except that CoCl_2 (5 mM) was added to 40 ml of crude extract instead of iron. The iron content was determined using ferrozine ($\epsilon_{565\text{ nm}} = 27900\text{ M}^{-1}\cdot\text{cm}^{-1}$) (33), and protein concentration was determined spectrophotometrically as described previously (9). The concentration of cobalt was determined by EPR titration (see below). Samples for MCD spectroscopy were prepared by dilution of reduced GAF_{NorR} in one volume of deuterated glycerol.

Iron Dissociation Rates—The dissociation rate of the iron complex in NorR was estimated using competition between NorR-Fe(II) and ferrozine (34, 35). An excess of ferrozine (final

concentration, 4 mM) was added in a gas-tight Hamilton syringe to NorR and mutant preparations (8–16 μM in 100 mM Tris-HCl, pH 8.5, 100 mM NaCl, 40% glycerol), and the rate of Fe(II)-ferrozine formation was monitored under anaerobic conditions at 565 nm.

Oxidation and NO Treatment of Iron-containing Proteins—Anaerobically purified GAF_{NorR} and mutant NorR proteins were oxidized by exposing these solutions to air for 2 h. Anaerobically purified NorR was oxidized by reaction with 5 equivalents of hydrogen peroxide for 30 min. Stock solutions of MAHMA NONOate were prepared in 10 mM NaOH. NO solutions were prepared by decomposition of a solution of MAHMA NONOate in 100 mM Tris-HCl, pH 8.5, 100 mM NaCl, 5% glycerol at 30 °C for 20 min ($t_{1/2} = 3$ min, pH = 7.5, 30 °C) under anaerobic conditions. Samples for UV-visible and EPR spectroscopy were prepared by reaction of anaerobically purified NorR, GAF_{NorR} , R81L, D99A, and H111L with 5 equivalents of NO from pre-decomposed MAHMA NONOate under anaerobic conditions.

Spectroscopic Methods—X-band EPR spectra were recorded on a Bruker ELEXSYS 500 instrument and a Bruker Super-High-Q Cavity: ER 4122SHQE. Temperature-dependent experiments were performed with an Oxford Instruments ESR-9 flow cryostat. EPR spin quantification was achieved by measurement of the total area of the absorption spectrum or integration of simulated EPR spectra or integration of the low field “absorption shaped” feature, using the method of Aasa and Vänngård (36). 1 mM aqueous $\text{Cu}(\text{II})(\text{H}_2\text{O})_6$ was used as the concentration standard. *E/D* ratios were calculated as described previously (37). EPR spectra were simulated using WINEPR SimFonia v. 1.25 (Bruker Analytische Messtechnik GmbH). Electronic absorption spectra were recorded on a PerkinElmer Life Sciences Lambda 35 spectrophotometer. MCD spectra were recorded on a circular dichrograph (JASCO J-730).

Structural Modeling—A homology model of the GAF domain of NorR was built using InsightII. Both phyre and Metaserver (38) were used to search for a suitable template; both servers returned the GAF B domain of the regulatory segment of mouse 3',5'-cyclic nucleotide phosphodiesterase (PDB ID 1MC0) as the best hit. An initial working model was developed using the Homology module of InsightII, and sequence alignment was returned by phyre. An iron atom was imported to the structure and placed at a bonding distance from S^γ -Cys-113. The sequence alignment returned by phyre was slightly adjusted in order to bring Asp-131 close to the iron binding site, which was tentatively assigned to a location equidistant from the S^γ of Cys-113 and O^δ of Asp-99. Several homology models were generated with different combinations of candidate ligands with Asp-99 as mono-dentate and Asp-96 and Asp-131 as either mono- or bi-dentate ligands. These models were then optimized by using the steepest descent or conjugate algorithm under a variety of structural constraints. In a typical optimization protocol the entire molecule was fixed except the iron atom and its coordinating residues, which were allowed to move freely and acquire any conformation that satisfied the imposed constraints of 1.8–2.0 Å for the Fe–O and 1.8–2.3 Å for the Fe–S bonds. After every minimization step ($\sim 10^4$ to 10^6

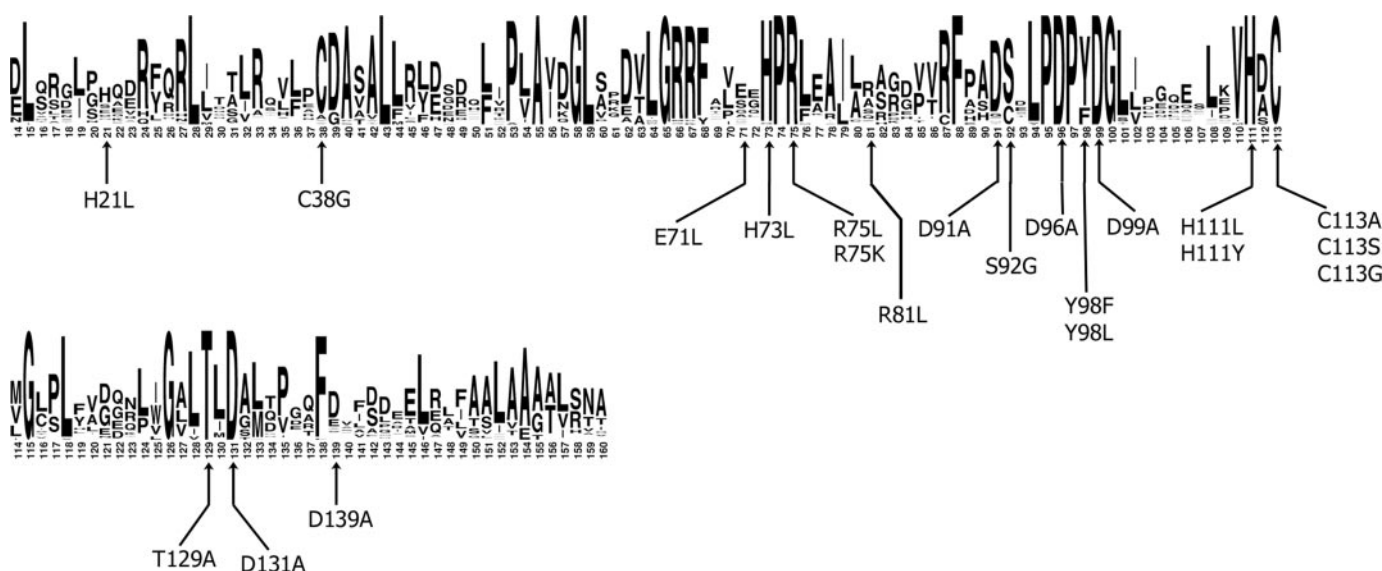


FIGURE 1. **Sequence logo** derived from alignment of 34 NorR GAF domains using Weblogo software. Residues are numbered with respect to *E. coli* NorR and mutations characterized in this study are listed beneath the logo.

iterations), the structural statistics, particularly chirality, Ramachandran plot, and omega values were checked. Final minimization always involved a constraints free optimization to check if the resulting structure maintained the established iron coordination.

RESULTS

Site-directed Mutagenesis of the GAF Domain of NorR

Analysis of the N-terminal GAF domains of 34 presumed NorR orthologues revealed several conserved residues that may act as ligands to the mononuclear non-heme iron center (Fig. 1). As noted by others (19), two histidine residues and a cysteine residue (located at positions 73, 111, and 113, respectively, in *E. coli* NorR) are invariant in NorR proteins; in contrast Cys-38 and His-21 are less well conserved in NorR homologues. We chose to mutate each of these histidine and cysteine residues (Fig. 1). We also noticed that NorR contains three conserved aspartate residues at positions 96, 99, and 131 that may bind a metal ion. We previously reported that a D99A substitution abolished the *in vivo* activity of NorR, and the whole cell $g = 4$ EPR signal is characteristic of the mononitrosyl-iron complex (9). It is therefore of interest to analyze the function of the other aspartate residues in the GAF domain. Guided by a structural model of the N-terminal domain of NorR based upon known GAF domain structures (see below), we also chose to mutate the conserved residues Arg-75 and Tyr-98. In some cases, we substituted more than one amino acid at a given position to fully investigate side-chain functions. In total we constructed the 21 substitutions shown in Fig. 1.

In Vivo Activities of NorR Mutant Proteins

Mutants were assayed for transcriptional activation of the *norVW* promoter using a single copy chromosomal *norV-lacZ* fusion introduced into a Δ *norR* background and complemented by pET-derived constructs carrying the mutant *norR* genes. Expression in this system relies upon low level transcription of genes cloned in pET plasmids when T7 RNA polymerase is not

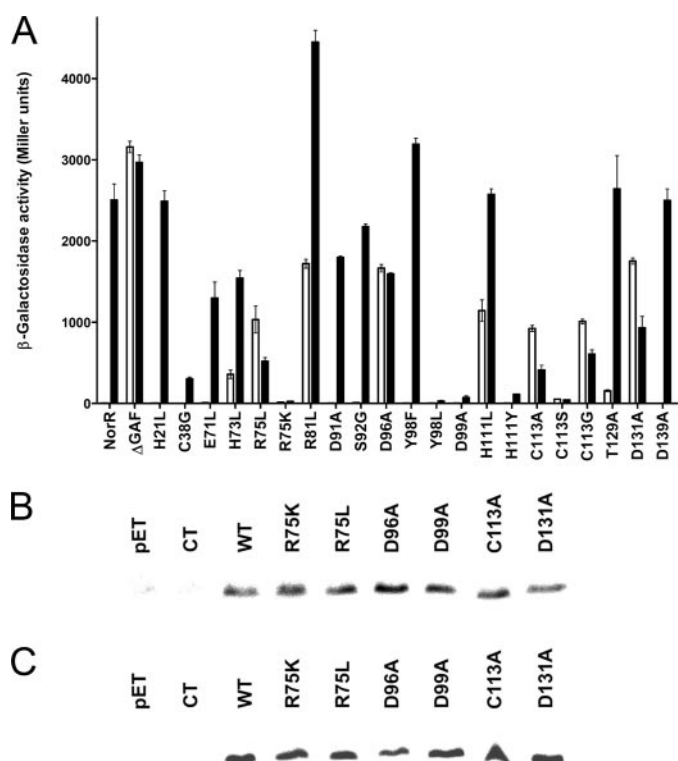


FIGURE 2. **Transcriptional activation *in vivo* by NorR and mutant derivatives and stability of mutant proteins.** A, activation of *norV-lacZ* expression *in vivo* by plasmids encoding NorR, NorR Δ GAF, or NorR mutants. Values represent the mean of at least three independent determinations. Cultures were grown either in the absence (open bars) or presence (closed bars) of potassium nitrite. B, Western blots of NorR and mutant derivatives in strains grown under the same conditions as used for the β -galactosidase assays in the absence of potassium nitrite. pET indicates vector alone; CT indicates strain NPT1003 lacking NorR. C, Western blotting as in B but strains were grown in the presence of potassium nitrite.

expressed (39). Potassium nitrite was used as a terminal electron acceptor to provide an endogenous source of NO to induce activation of NorR (20). Mutant proteins fell into three distinct classes on the basis of these results (Fig. 2). First, NorR variants

TABLE 1
Summary of the properties of mutant proteins

Protein	Class	<i>In vivo</i> EPR ^a	Iron content ^b after reconstitution (heparin)	Iron dissociation rate k_{off}	<i>In vitro</i> EPR <i>g</i> values
				s^{-1}	
NorR	Wildtype	+	0.88 ± 0.08	0.02	4.21, 3.82, 2.00
H21L	I (wild type)	ND ^c	ND	ND	ND
C38G	I (wild type)	+	ND	ND	ND
E71L	I (wild type)	ND	ND	ND	ND
H73L	I (wild type)	ND	ND	ND	ND
R75K	III (null)	*	0.90 ± 0.04	1.17	
R75L	II (constitutive)	*	0.73 ± 0.16	2.13	
R81L	II (constitutive)	+	0.50 ± 0.09	ND	4.21, 3.82, 2.00
S92G	I (wild type)	+	ND	ND	ND
D96A	II (constitutive)	—	0.35 ± 0.12	2.49	
Y98F	I (wild type)	+	0.86	0.03	4.17, 3.92, 2.00
Y98L	III (null)	+	0.87 ± 0.08	0.07	(A) 4.49, 3.53, 2.00 (B) 4.12, 3.95, 2.00
D99A	III (null)	—	0.28 ± 0.11	ND	4.28, 3.76, 2.00
H111Y	III (null)	—	ND	ND	ND
H111L	II (constitutive)	+	0.5 ± 0.10	ND	ND
C113G	II (constitutive)	—	0.07 ± 0.03	ND	
C113A	II (constitutive)	—	0.06 ± 0.01	ND	
C113S	III (null)	—	0.05 ± 0.03	ND	
T129A	I (wild type)	+	ND	ND	ND
D131A	II (constitutive)	—	0.33 ± 0.02	2.11	
D139A	I (wild type)	ND	ND	ND	ND

^a The presence of $g = 4$ EPR signal in cultures expressing NorR after NO exposure; +, signal intensity equivalent to wild-type NorR; *, signal intensity less than 2.5% of wild-type NorR; —, EPR signal undetectable.

^b Iron content expressed as atoms per monomer after iron reconstitution and purification by heparin affinity chromatography. Where indicated, standard deviations were determined from at least two independent reconstituted protein preparations.

^c ND, not determined.

that did not exhibit major differences compared with the wild-type protein (Class I); these include E71L, H73L, D91A, S92G, T129A, and D139A, which were not studied further. The silent phenotype of Y98F was not unexpected, because tyrosine is replaced by phenylalanine at this position in several NorR proteins. The C38G protein exhibited a lower level of activity in the presence of nitrite than the wild type (Fig. 2). Nevertheless it is unlikely that Cys-38 is a ligand to the ferrous iron center as C38G gave a normal whole cell EPR signal (see below and Table 1). Members of the second class of variants were able to activate the *norVW* promoter in the absence of inducer (Class II). This was a surprisingly large group with one variant, D96A, exhibiting constitutive activity similar to that of a truncated version of NorR lacking the GAF domain (NorRΔGAF) (9), whereas others displayed greater activity either in the presence (e.g. R81L and H111L) or absence (e.g. R75L, C113A, C113G, and D131A) of inducer (Fig. 2). The third class of mutations (Class III) eliminated transcriptional activation by NorR and the response to NO; these include R75K, Y98L, D99A, H111Y, and C113S. A notable outcome of this analysis is that different substitutions of the same residue gave rise to remarkably different phenotypes, for example, R75L is constitutive whereas R75K is inactive. These differences do not appear to relate to stability, because all the mutant proteins were expressed at similar levels under these growth conditions either in the absence or presence of inducer, as assessed by Western blotting (Fig. 2, B and C). Instead, these differences seem to correlate with the hydrophobic nature of the residue, because the R75L, H111L, and C113A proteins are constitutive, whereas the corresponding R75K, H111Y, and C113S substitutions have null phenotypes. In addition, most of the other hydrophobic substitutions (H73L, R81L, D96A, and D131A) lead to a constitutive phenotype.

Whole Cell EPR

We previously reported that the EPR signal of NO-bound NorR can be detected in anaerobic cultures of *E. coli* induced for NorR expression and subsequently treated with NO (9). Derivative signals at $g = 4.21$ and 3.88 are characteristic of the $\{\text{Fe}(\text{NO})\}^7$ complex in NorR and provide an indirect method to probe for the presence of the non-heme iron center *in vivo* (Fig. 3A, *spectrum 1*). We analyzed the EPR spectra of whole cells induced for expression of the mutant proteins prior to and after treatment of the cells with the NO donor MAHMA NONOate. All the mutant proteins were expressed at similar levels to the wild-type NorR (data not shown). We observed that cultures expressing the H73L, D91A, S92G, and T129A proteins exhibited the characteristic $g = 4$ EPR signal after exposure to the NO donor, with g values identical to those of wild-type NorR (data not shown), in agreement with their *in vivo* activities. Although the C38G mutant gave a relatively low level of transcriptional activation in the presence of inducer (Fig. 2), cultures expressing this protein gave rise to EPR signals identical to wild type (data not shown). The constitutive mutants R81L and H111L also exhibited *in vivo* EPR signals identical to those of wild type as anticipated from their response to inducer in the *in vivo* activation assays (Fig. 2). The Y98F mutant gave rise to a slightly less rhombic EPR signal than the wild type, with derivative signals at $g = 4.17$ and $g = 3.92$ (Fig. 3A, *spectrum 2*). In contrast, the inactive Y98L mutant gave rise to a complex signal indicative of a mixed species (Fig. 3A, *spectrum 3*). A very weak EPR signal characteristic of the mononitrosyl-iron complex was detectable in cultures expressing the R75K and R75L mutant proteins after exposure to NO. The $g = 4.2$ EPR signal was entirely absent in NO-treated cultures expressing the D96A, D99A, H111Y, C113A, C113S, C113G, and D131A proteins, and their features were similar to wild-type NorR in the absence of NO (Fig. 3A, *spectrum 4*). These results suggest

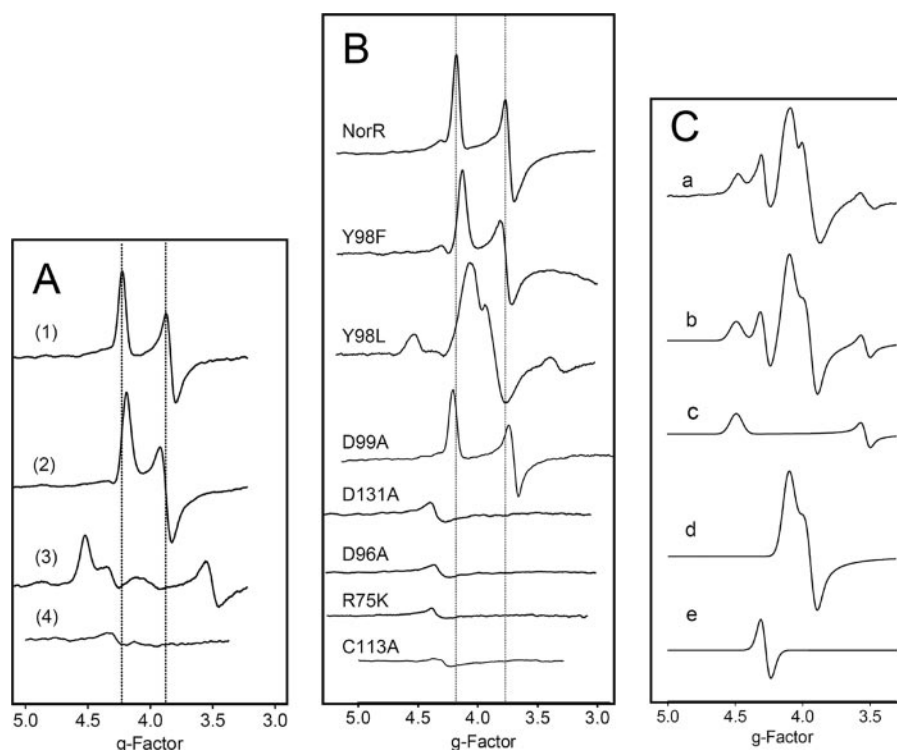


FIGURE 3. X-band EPR spectra of whole cells and purified proteins. A, EPR spectra recorded from *E. coli* BL21(DE3) cultures expressing NorR (spectrum 1 and 4), Y98F (spectrum 2), and Y98L (spectrum 3). Spectra 1–3 were obtained from cultures exposed to the NO donor MAMHA NONOate. The culture used to record spectrum 4 was not exposed to NO. B, EPR spectra of purified proteins reconstituted with Fe(II) (final protein concentration, 7–16 μM) treated with 10 equivalents of NO from MAMHA NONOate. EPR spectra were recorded under the following conditions: frequency, 9.440 GHz; power, 2 milliwatts; modulation amplitude, 10 G; modulation frequency, 100 kHz; temperature, 8 K. C, simulation of the Y98L EPR spectrum. a, experimental spectrum; b, complete simulation; c, simulation of species A with $g_{1,2,3} = 4.49, 3.53, \text{ and } 2.00$; d, simulation of species B with $g_{1,2,3} = 4.12, 3.95, \text{ and } 2.00$; e, simulated adventitious iron, representing 0.5% of the total iron signal.

that either these mutants lack a functional non-heme iron center, or possibly that NO is unable to access the center.

Iron Content of Purified Proteins

Wild-type and mutant NorR proteins were purified under anaerobic conditions as described previously (9). NorR retains ~ 0.3 atoms of iron when purified under these conditions, but ferrous iron can be reconstituted into the protein to yield ~ 0.9 iron atoms per monomer (9). Using the ferrozine assay we estimate a dissociation rate constant (k_{off}) of 0.02 s^{-1} for the ferrous iron in reconstituted NorR. In the absence of reconstitution, most of the purified mutant proteins were devoid of iron. When ferrous iron was added in the crude extract prior to the purification, we found that many of the mutant proteins also lacked ferrous iron after the final chromatography step on Superdex 200. All mutants and the wild-type protein eluted at a retention volume, $V = 63 \text{ ml}$, on gel-exclusion chromatography, corresponding to a molecular mass of 150 kDa, consistent with a trimeric structure (data not shown). However, many of the mutant proteins retained some iron after the first step of the purification (the heparin column) (Table 1). These results suggest that, although most of the mutant proteins are competent to bind iron, it is lost during purification. In some cases this may explain the absence of signals attributable to an Fe(NO) complex in the whole cell EPR experiments.

EPR and UV-visible Spectroscopies

The absence of iron in many of the mutant proteins after purification to homogeneity precluded spectroscopic analysis. However, because some iron was retained after reconstitution in the crude extract and subsequent chromatography on heparin-Sepharose, it was possible to examine the spectroscopic features of mutant proteins after heparin chromatography. The protein preparations examined in these experiments were $>95\%$ pure as judged by Coomassie-stained gels. The properties of wild-type NorR and the mutant proteins are discussed individually below and are summarized in Table 1.

NorR—The electronic absorption spectrum in the UV-visible domain of reduced NorR-Fe(II) was dominated by the absorption of aromatic amino acid residues at $\lambda_{\text{max}} = 280 \text{ nm}$. When incubated with NO the protein solution immediately turned yellow and displayed absorption bands with $\lambda_{\text{max}} 435 \text{ nm}$ characteristic of nitrosyl-iron complexes and attributed to LMCT $\text{NO}^- \rightarrow \text{Fe}^{3+}$ (Fig. 4A). A very similar spectrum was obtained when the iron-

reconstituted isolated GAF domain of NorR ($\text{GAF}_{\text{NorR}}\text{-Fe(II)}$) was exposed to NO (Fig. 4A). As reported previously, when exposed to NO, NorR exhibited strong EPR signals with characteristic g values at 4.21, 3.82, and 2.00 ($E/D \approx 0.03$, where D and E are the axial and rhombic zero-field splitting parameters, respectively), that represent the $\{\text{Fe(NO)}\}^7$ ($S = 3/2$) complex (Fig. 3B).

We reported previously that the ferrous iron in wild-type full-length NorR was stable to air (9). In an attempt to generate a ferric state in full-length NorR, the protein was incubated with 5 equivalents of hydrogen peroxide. The EPR spectra of H_2O_2 -treated NorR displayed derivative signals characteristic of a high spin non-heme ferric iron ($S = 5/2$) at around $g = 4.3$ and a signal at $g = 9.5$ only seen at temperatures below 5K. Computer simulation returned $E/D \approx 0.31$, indicating the symmetry at the ferric iron center was very low. In contrast, identical EPR signals were obtained when $\text{GAF}_{\text{NorR}}\text{-Fe(II)}$ was exposed to air, indicating that the ferrous iron center in the isolated GAF domain of NorR is far more sensitive to oxidation than in full-length NorR (data not shown).

The UV-visible spectrum of H_2O_2 -treated NorR (Fig. 4B) exhibited a broad band with maximum at 300 nm and an absorption coefficient $\epsilon = 1800 \text{ M}^{-1}\text{cm}^{-1}$ typical of a charge transfer transition. Oxidized GAF_{NorR} exhibited a similar spectrum with an adsorption maximum at 310 nm. High spin ferric

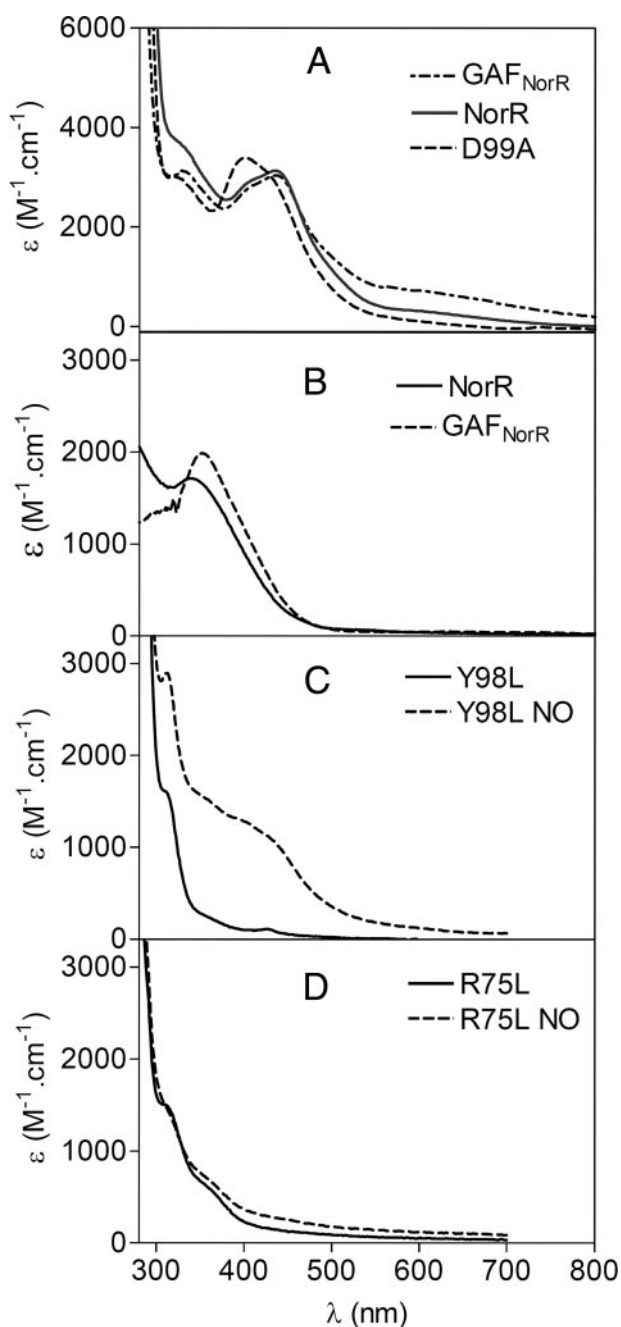


FIGURE 4. Electronic absorption spectra of NorR and mutant derivatives. A, electronic absorption spectra of NorR, GAF_{NorR} , and D99A in their reduced state and treated with 10 equivalents of NO from MAMHA NONOate. Calculation of the absorption coefficients was based on the iron content of the proteins as listed in Table 1. B, oxidized-reduced difference spectra of NorR (solid line) and GAF_{NorR} (dotted line). NorR (150 μ M) was exposed to 5 equivalents of H_2O_2 for 30 min to achieve oxidation, whereas GAF_{NorR} (400 μ M) was exposed to air for 2 h. Calculation of the absorption coefficients was based on the iron content of NorR and GAF_{NorR} : 0.9 and 0.7 iron atom/monomer, respectively. C, absorption spectra of iron-reconstituted Y98L in the absence of NO (solid line) or treated with 10 equivalents of NO as in panel A (dotted line). D, absorption spectra of iron-reconstituted R75L in the absence of NO (solid line) or treated with 10 equivalents of NO as in panel A (dotted line).

iron enzymes and inorganic complexes usually display LMCT bands between 300 and 500 nm with nitrogen donor atoms provided by amine or imidazole groups and oxygen donors by carboxylate groups. Commonly, a LMCT band of (His)N \rightarrow Fe^{3+} is generally observed at around 350 nm (40–43). The

band at 300 nm for NorR is indicative of ligation by nitrogen and/or oxygen donor atoms and possibly histidine and/or aspartate/glutamate. Tyrosine can be ruled out, as we would expect an intense absorption around 500–600 nm ($\epsilon \approx 3000$ $M^{-1} \cdot cm^{-1}$) due to the (Tyr)O $^- \rightarrow Fe^{3+}$ LMCT transition (40, 44, 45).

R81L and H111L—The electronic absorption spectra and EPR spectra of the reduced forms of these proteins were identical to those of wild-type NorR (data not shown). However, in contrast to wild-type NorR, both proteins were sensitive to oxidation in air and displayed the spectral features of H_2O_2 -treated NorR after a short exposure to oxygen.

D99A—Although this mutant protein did not exhibit an EPR signal in whole cells, it was possible to reconstitute iron into this protein to 0.28 atom per monomer (Table 1). The UV-visible spectrum of the reduced form of D99A after NO treatment was different from wild-type NorR with an absorption maximum of 400 nm rather than 435 nm (Fig. 4A). The EPR spectrum of NO-treated D99A displayed derivative signals at $g = 4.28$, 3.76, and 2.00 ($E/D \approx 0.05$) that were characteristic of a mononitrosyl-iron complex $\{Fe(NO)\}^7$ ($S = 3/2$), but associated with a more rhombic symmetry than the wild-type NorR-Fe(NO) (Fig. 3B). The non-heme iron center in the reconstituted D99A protein was also more sensitive to air exposure than wild-type NorR.

D96A and D131A—These mutant proteins retained similar levels of iron to D99A after heparin chromatography. However, the ferrous iron was apparently far more accessible to ferrozine than in the wild-type NorR with off-rates for the iron of 2.49 s^{-1} for D96A and 2.11 s^{-1} for D131A, respectively (Table 1). These mutant proteins did not form a mononitrosyl-iron complex after exposure to NO, as evidenced by the absence of the $g = 4$ EPR signal (Fig. 3B) and the absorption peak at 430 nm (data not shown).

C113A and C113S—These mutants were distinguishable by the absence of absorption bands around 430 nm after exposure to NO and the absence of EPR signals corresponding to the $\{Fe(NO)\}^7$ ($S = 3/2$) complex (data for C113A are shown in Fig. 3B), as anticipated from the *in vivo* EPR data and the absence of iron (Table 1).

Y98F and Y98L—These proteins had properties in accordance with their EPR spectral features *in vivo*. The amount and stability of the ferrous iron in these proteins was similar to that of wild-type NorR with off-rates of 0.03 s^{-1} for Y98F and 0.07 s^{-1} for Y98L (Table 1). Both mutant proteins exhibited absorption maxima at ~ 420 nm after exposure to NO. Y98F displayed a less rhombic EPR signal, as observed *in vivo* after exposure to NO, with $g = 4.17$, 3.92, and 2.00 ($E/D \approx 0.02$) (Fig. 3B). The EPR features of NO-treated Y98L were complex and indicative of two overlapping $S = 3/2$ species. One of these components (signal A) has a more rhombic resonance than wild type NorR with $g = 4.49$, 3.53, and 2.0, with $E/D = 0.08$. The second species (signal B) displays a more axial resonance with $g = 4.12$, 3.95, and 2.0, with $E/D = 0.02$. Comparison of the signal intensities with a $Cu(II)(H_2O)_6$ standard indicated that the total resonance corresponded to $\sim 62\%$ of the iron in NorR. Simulation of the spectrum and comparison of the total integrals from each species indicated that at a high NO:NorR stoichiometry (10:1), the A and B components were present at a ratio of 1:2 (Fig. 3C).

NorR Iron Center

The intensity of the rhombic component with $E/D = 0.08$ (signal A) remained relatively constant with respect to the NO concentration, whereas the axial component (signal B) decreased in intensity at lower NO:NorR ratios (data not shown). It is notable that signal A is the major species detected *in vivo* (Fig. 3A), perhaps reflecting lower concentrations of NO within whole cells.

R75K and R75L—After heparin chromatography, these proteins retained similar levels of ferrous iron to wild-type NorR, but the iron was less stable in these proteins with off-rates of 1.17 s^{-1} for R75K and 2.13 s^{-1} for R75L, respectively (Table 1). Although a very weak EPR signal characteristic of the $\{\text{Fe}(\text{NO})\}^7$ ($S = 3/2$) complex was detectable *in vivo*, no corresponding $g = 4$ signal was observed with purified iron-reconstituted proteins exposed to NO. In addition the characteristic 430 nm peak in the visible absorption spectrum attributed to $\text{NO}^- \rightarrow \text{Fe}^{3+}$ LMCT was absent. (Data for R75L are shown in Figs. 3B and 4D.)

Cobalt-substituted NorR

Cobalt ion, Co^{2+} , was used as a structural probe of the NorR iron center. The low temperature EPR spectrum of Co^{2+} -substituted NorR displayed derivative signals at $g_{\text{eff}(x,y,z)} = 5.35$, 3.65, and 1.95 at 5K, indicating that the cobalt is high spin $\text{Co}(\text{II})$ ($S = 3/2$) (Fig. 5). The EPR signals at $g = 2$ probably arise from copper contaminants and the feature around $g = 4.3$ from adventitious ferric iron. Computer simulation returned spin Hamiltonian parameters for the ground state $M_s = |\pm 1/2\rangle$, $E/D = 0.15$ (3), $g_{\text{real}(x,y)} \approx 2.4$, and $g_{\text{real}(z)} \approx 2.1$. Six coordinate complexes generally exhibit low E/D due to a high degree of axial symmetry. The parameters of NorR- $\text{Co}(\text{II})$ are indicative of either five- or six-coordinate cobalt in a distorted octahedral symmetry (46–48).

Some empirical rules have been established for electronic absorption spectra of $\text{Co}(\text{II})$ complexes based on comparison with several enzymes and inorganic complexes. The ligand field $d-d$ features are observed in the 450–700 nm region, and complexes exhibiting extinction coefficients $>300 \text{ M}^{-1} \cdot \text{cm}^{-1}$ are generally four-coordinate, those in between $300 \text{ M}^{-1} \cdot \text{cm}^{-1}$ and $50 \text{ M}^{-1} \cdot \text{cm}^{-1}$ are five-coordinate, and those lower than $50 \text{ M}^{-1} \cdot \text{cm}^{-1}$ are six-coordinate (49, 50). In addition, specific features of cysteine are found at around 320–350 nm due to LMCT ($\text{CysS}^- \rightarrow \text{Co}^{2+}$), with absorption coefficients between $900 \text{ M}^{-1} \cdot \text{cm}^{-1}$ and $1400 \text{ M}^{-1} \cdot \text{cm}^{-1}$ at 320 nm for one cysteine coordinated (51–53). The full-length NorR was reconstituted with Co^{2+} ion. The UV-visible difference spectra of Co^{2+} -substituted NorR and apo-NorR displayed one intense band at 315 nm ($\epsilon = 1600 \text{ M}^{-1} \cdot \text{cm}^{-1}$) and two shoulders at 360 nm and 410 nm, as well as several less intense bands between 500 and 700 nm with maxima at 590 nm ($\epsilon = 95 \text{ M}^{-1} \cdot \text{cm}^{-1}$) and several shoulders at 520, 610, and 680 nm (Fig. 6). The latter bands were assigned to ligand field $d-d$ transitions, and absorption coefficients were consistent with an intermediate 5/6 coordinate complex in distorted octahedral geometry. The intense band at 315 nm may be assigned to a LMCT transition ($\text{CysS}^- \rightarrow \text{Co}^{2+}$), and the absorption coefficient was consistent with the coordination of a single cysteine residue.

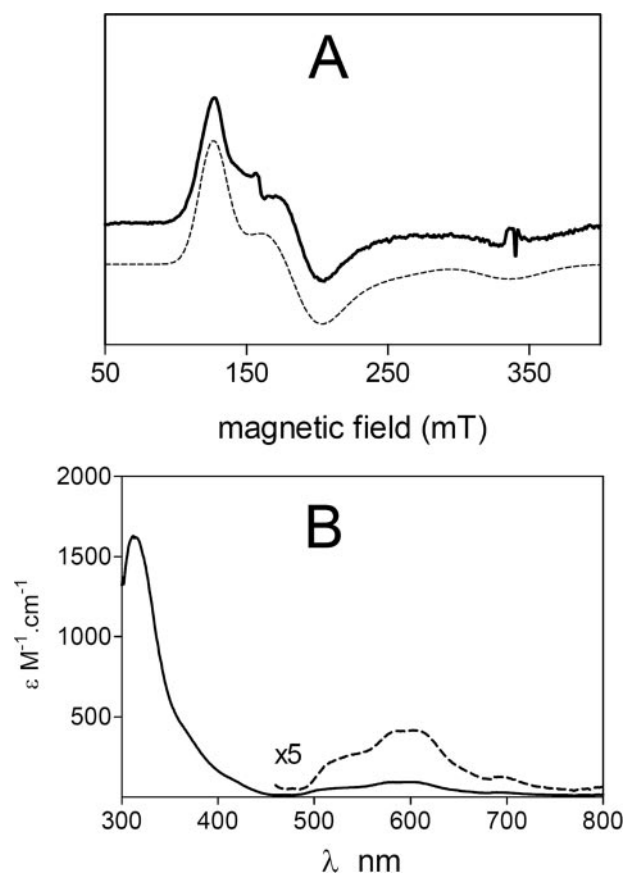


FIGURE 5. Spectroscopic properties of Co^{2+} -substituted NorR. A, EPR spectrum of Co^{2+} -substituted NorR ($400 \mu\text{M}$) recorded at 4.2 K. The dotted sub-spectrum represents a simulation with the following parameters: $g_{\text{eff}(x,y,z)} = 5.35$, 3.65, and 1.95, and the respective line widths of 20, 30, and 55 mT. EPR spectra were recorded under the following conditions: frequency, 9.477 GHz; power, 1 milliwatt; modulation amplitude, 10 G; modulation frequency, 100 kHz; temperature 4.2 K. B, electronic absorption difference spectrum of Co^{2+} -substituted NorR-apoNorR. The protein concentration was $400 \mu\text{M}$, and the amount of cobalt incorporated ($320 \mu\text{M}$) was used to determine the absorption coefficients, as estimated from the EPR titration. The dotted sub-spectrum is a 5-fold expansion of the 450–700 nm region to show the ligand field $d-d$ features.

MCD Spectroscopy

The UV-visible spectrum of iron-reconstituted GAF_{NorR} in the reduced state, $\text{GAF}_{\text{NorR}}\text{-Fe}(\text{II})$, was dominated by the intense absorption at $36,000 \text{ cm}^{-1}$ arising from aromatic amino acid residues, and the features attributable to CT transitions may be hidden by this band. However, MCD facilitates investigation of CT transitions by selectively investigating the electronic transitions associated with the paramagnetic Fe^{2+} active site. The MCD spectrum of $\text{GAF}_{\text{NorR}}\text{-Fe}(\text{II})$ displayed two positive terms at $35,300 \text{ cm}^{-1}$ ($\Delta\epsilon = 90 \text{ M}^{-1} \cdot \text{cm}^{-1}$) and $38,000 \text{ cm}^{-1}$ ($\Delta\epsilon = 100 \text{ M}^{-1} \cdot \text{cm}^{-1}$), with absorption coefficients consistent with CT transitions (Fig. 6). Similar positively signed transitions at $31,200 \text{ cm}^{-1}$ ($\Delta\epsilon = 90 \text{ M}^{-1} \cdot \text{cm}^{-1}$), $33,900 \text{ cm}^{-1}$ ($\Delta\epsilon = 110 \text{ M}^{-1} \cdot \text{cm}^{-1}$), and $38,900 \text{ cm}^{-1}$ ($\Delta\epsilon = 40 \text{ M}^{-1} \cdot \text{cm}^{-1}$) in the VT-MCD spectra of reduced *Pyrococcus furiosus* superoxide reductase were tentatively assigned to $(\text{Cys})\text{S}^- \rightarrow \text{Fe}^{2+}$ (54).

Structural Modeling of the Non-heme Ferrous Iron Center

The GAF domain of NorR was modeled on the x-ray structure of the regulatory GAF-B domain of 3',5'-cyclic nucleotide

phosphodiesterase 2a, which binds cGMP (PDB code 1MC0 (55)). The location of the ferrous iron was modeled *ab initio* without reference to the cGMP heteroatoms in the 1MC0 template. The assignment of the iron site was based upon the properties of NorR mutants, and candidate ligands that gave rise to no phenotypic change when substituted were discounted. The absence of a (Tyr)O⁻ → Fe³⁺ LMCT transition and the silent phenotype of Y98F ruled out tyrosine as a potential ligand. The iron was positioned within bonding distance of Cys-113 based upon the results of the site-directed mutagenesis and the (Cys)S⁻ → Co²⁺ LMCT observed with the cobalt-substituted

protein. After extensive optimization, two models were developed that had very similar iron binding sites defined by Arg-75, Asp-96, Tyr-98, Asp-99, His-111, Asp-113, and Asp-131 but differed in whether Arg-75 was a coordinating or a non-coordinating ligand of the iron atom. One of these models contains penta-coordinated iron, which is optimized in a trigonal bipyramidal geometry, and left Arg-75 out of the first coordination shell of the Fe. The second model brought Arg-75 to the coordination fold of the iron atom and resulted in a hexa-coordinated metal ion center with distorted octahedral geometry (Fig. 7). Although the coordination geometry of the iron atom in the two models is different, the overall environment of the iron atom remains the same, and hence activity modulation triggered by the site-directed mutagenesis can be rationalized. We favor the hexa-coordinate model (Fig. 7B), because it is consistent with the coordination geometry suggested by the spectroscopic features of cobalt-substituted NorR. Overall the iron center is located in a similar location to that of cGMP in PDE2 and is likely to be excluded from contact with solvent by the protein. As anticipated, substitutions that had little influence on protein activity (E71L, H73L, D91A, S92G, T129A, D139A, and C38G) are located in residues that are not predicted to influence the active site. His-111 is predicted to be an active site residue, as its side chain bends toward the iron atom, but is not directly bonded to it. Arg-81 is located on the protein surface (Fig. 7A), and thus the constitutive phenotype of the R81L mutation may arise from defects in inter-domain interactions. Tyr-98 is predicted to occupy a prominent position between the two coordinating residues Asp-96 and Asp-99 and may also play a role in defining the active site.

DISCUSSION

In the absence of NO, NorR is maintained in an inactive state as a consequence of intramolecular repression of the AAA+ domain by the sensory GAF domain. We have proposed that, when NO interacts with the iron center in the GAF domain to generate a mononitrosyl {Fe(NO)}⁷ complex, the conformation of the GAF domain alters, thus relieving repression of the AAA+ domain and enabling transcriptional activation by NorR (9). Apart from silent mutations (Class I), the substitutions we have introduced into the GAF domain produce NorR proteins that predominately fall into two classes, those with constitutive activity (Class II), which are defective in intramolecular repression, and inactive proteins (Class III) that are defective in transcriptional activation.

A constitutive phenotype could arise either as consequence of a perturbation of GAF-AAA+ domain interactions, a conformational change in the GAF domain similar to that of the activated form or a change in the coordination environment of the ferrous iron that mimics the NO-activated state. It is particularly striking that hydrophobic substitutions lead to a constitutive

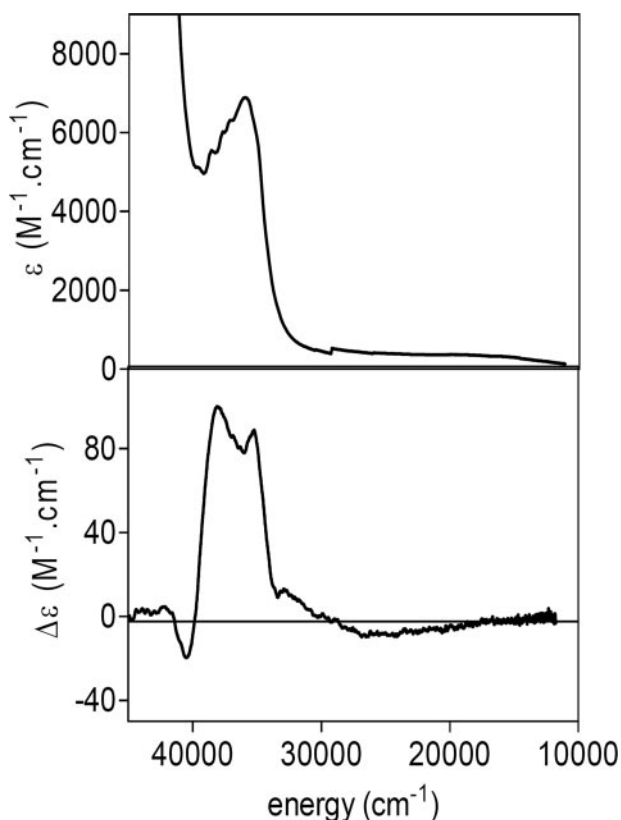


FIGURE 6. **Electronic absorption and MCD spectra of reduced GAF_{NorR}.** Top, electronic absorption spectrum of reduced GAF_{NorR} (500 μM) in anaerobic conditions. Bottom, MCD spectrum of reduced GAF_{NorR} (500 μM, 50% deuterated glycerol) recorded in anaerobic conditions.

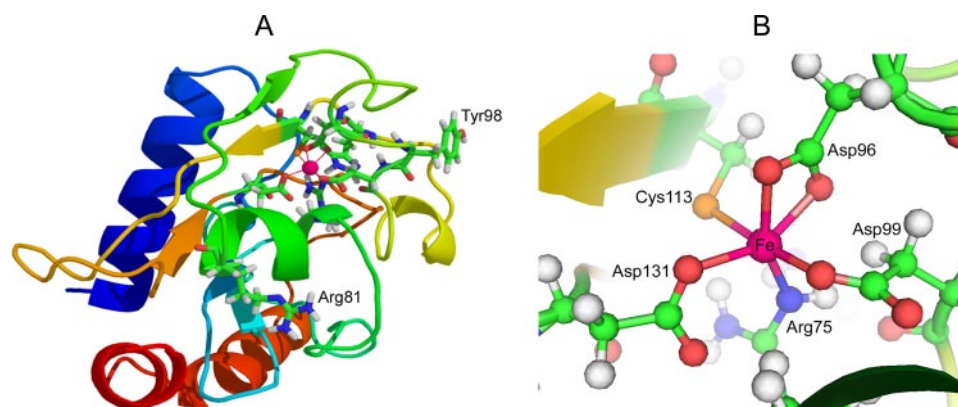


FIGURE 7. **Structural model of the ferrous iron center in the GAF domain of NorR.** A, overview of the model showing the position of the iron in the domain and the locations of Arg-81 and Tyr-98. B, view of the ferrous iron center showing the proposed iron ligands.

phenotype and that the *in vivo* activities of mutant proteins with hydrophobic substitutions in residues predicted to be iron ligands (R75L, C113A, C113G, and D131A) are negatively influenced by the presence of NO. Our molecular model places these residues in a relatively rigid portion of the iron binding site in which hydrophobic substitutions may yield an activated state of NorR, different to that attained in the wild-type protein. In contrast, the D96A substitution leads to a constitutive phenotype that is not influenced by the presence of NO, and this residue is predicted to reside in a more flexible region of the active site.

Two other constitutive mutations, R81L and H111L, had entirely different properties. These substitutions do not appear to disrupt the iron center, because the proteins exhibited EPR spectral features characteristic of the Fe(NO) complex identical to those of wild-type NorR, both *in vivo* and *in vitro*. Moreover, transcriptional activation by the mutant proteins was enhanced by the presence of nitrite *in vivo*, suggesting that the presence of NO further decreases intramolecular repression by the GAF domain. Neither of these residues is therefore a candidate ligand to the iron. It is notable, however, that the ferrous iron is labile in these mutants, because the iron content was only 50% of the wild-type after heparin chromatography. Furthermore, the iron center in these mutant proteins was more sensitive to oxidation than wild-type protein. Our structural model predicts that Arg-81 lies on the surface of the GAF domain. A charged residue at this position might be important for GAF-AAA+ domain interactions in NorR, although this residue is not highly conserved in NorR proteins. In contrast to Arg-81, His-111 is predicted to be close to the coordinated iron and may function as part of a signal relay network that communicates the NO signal to influence interdomain interactions. A substitution in the equivalent residue (H110Q) in *Ralstonia eutropha* NorR is reported to increase the level of transcriptional activation 3-fold (56), again suggesting that the histidine at this position influences GAF-AAA+ domain interactions.

Null mutations could arise as a consequence of structural perturbations of the GAF domain, defects in signaling the NO response, or substitutions that influence iron coordination. We have previously demonstrated that apo-NorR is not competent to activate transcription (9), implying that intramolecular repression is maintained in the absence of the mononuclear ferrous iron center. Therefore all substitutions increasing iron lability by disruption of the intramolecular interactions between the GAF and AAA+ domains or through removal of an Fe²⁺ ligand could lead to a null phenotype. In many cases the ferrous iron in the mutant protein was more labile than in wild-type NorR. We also observed that the iron center in the isolated GAF domain of NorR is more sensitive to oxidation than full-length NorR suggesting that interdomain interactions may protect the iron center. In this study we observed that the iron center of some mutant proteins was more sensitive to oxidation than wild-type NorR.

Among the null mutations, the Y98L substitution is unique. The tyrosine residue at position 98 is conserved in many NorR sequences but is replaced by phenylalanine in, for example, some *Vibrio* species. Accordingly, the Y98F substitution was silent in *E. coli* NorR. Interestingly, EPR spectra of this mutant

protein exhibited derivatives characteristic of the Fe(NO) complex but with decreased rhombic symmetry, implying that the nature of the aromatic residue at this position influences the environment of the mononitrosyl-iron complex. In contrast, when the aromatic residue at position 98 was substituted by leucine, transcriptional activation by NorR was eliminated and the electronic properties of the Fe(NO) complex were altered, resulting in two overlapping $S = 3/2$ resonances. The more rhombic species with $E/D = 0.08$ appears to have a higher affinity for NO than the more axial EPR signal ($E/D = 0.02$), which increases at high NO:NorR ratios. Similar electronic heterogeneity has been observed in the $S = 3/2$ {Fe(NO)}⁷ complex of *P. furiosus* superoxide reductase. It has been suggested that the more rhombic resonance corresponds to a hexa-coordinated {Fe(NO)}⁷ complex, whereas the near axial species represents formation of a penta-coordinated iron-mononitrosyl species driven by NO-induced reversible cleavage of an Fe–S (Cys) bond (57). Potentially, the near axial species exhibited by the Y98L substitution in NorR, which is similar to the wild-type and Y98F spectra, might represent the activated “ON” state of NorR. In contrast to our results with *E. coli* NorR, the corresponding Y95L mutation in *R. eutropha* NorR retains the ability to activate transcription (58, 59). Although the contribution of the tyrosine to the {Fe(NO)}⁷ unit could be context-dependent, differences in the organism and culture conditions might lead to an increase in the axial species *in vivo* for Y95L in *R. eutropha* compared with Y98L in *E. coli*. Clearly however, tyrosine can be ruled out as a direct ligand to the ferrous iron since a (Tyr)O[−] → Fe³⁺ LMCT transition was not apparent in the optical absorption spectrum of oxidized NorR. Furthermore, as noted above, the Y98F mutation is silent with respect to transcriptional activation. Apparently, electron-rich aromatic rings appear to be a crucial requirement at this position.

Our results clearly demonstrate that the cysteine at position 38 and the two highly conserved histidine residues at positions 73 and 111, respectively, are not ligands to the iron. The UV-visible spectrum of cobalt-substituted NorR indicates that a single cysteine residue is a ligand to the metal ion, and the MCD data obtained with GAF_{NorR}-Fe(II) suggest the features in the UV domain at 35,300 cm^{−1} and 38,000 cm^{−1} may correspond to a (Cys)S[−] → Fe²⁺ LMCT transition. Because C38G is silent, cysteine 113 is therefore a very strong candidate for a ligand to the iron. All three proteins substituted at this position failed to bind iron, and we were unable to reconstitute ferrous iron into the mutant proteins *in vitro*. Accordingly none of these mutant proteins gave EPR signals in the presence of NO, indicative of the ferrous nitrosyl complex. The C113S substitution prevented transcriptional activation as reported for the equivalent mutation in *R. eutropha* NorR (56), whereas, as mentioned above, the C113A and C113G mutations activated transcription constitutively. Notably, H111Y also gives rise to a null phenotype. Possibly the hydroxyl groups on the tyrosine and serine residues of H111Y and C113S, respectively, may lock the protein in the inactive state.

The broad band with absorption max at 300 nm that we observe in the visible spectrum of oxidized NorR is typical of a nitrogen or oxygen donor atom in a ligand-Fe(III) CT transition. Our site-directed mutagenesis studies in combination

with structural modeling indicate that the ferrous iron in NorR is likely to be liganded by carboxylates from three conserved aspartate residues at positions 96, 99, and 131 (Fig. 7). We previously demonstrated that the D99A mutation abolished NO-dependent transcriptional activation by NorR and that iron was absent in the purified protein, commensurate with the lack of an EPR signal in whole cells exposed to NO (9). We have now demonstrated that it is possible to force reconstitution of iron into D99A, *in vitro*, but the amount of iron incorporated is relatively low (35%). The EPR and the UV-visible spectra of D99A showed that this mutation alters the structure of the Fe(NO) complex, suggesting that Asp-99 is a good candidate as a ligand to the iron. Similarly, we have been able to force reconstitution of iron into the D96A and D131A proteins, again to relatively low levels, but in these cases the mutant proteins do not exhibit EPR signals characteristic of the {Fe(NO)}⁷ (*S* = 3/2) complex. Therefore it would appear that these substitutions either severely disrupt the structure of the ferrous iron complex or prevent coordination of NO. As mentioned above, these substitutions also have a different phenotype to that of D99A in that transcriptional activation by NorR is constitutive. In contrast, Asp to Asn substitutions in equivalent positions in *R. eutropha* NorR inactivate the protein (59). At the early stages of structural modeling, it was realized that the side chain of Arg-75 could be constrained to reveal a covalent bond between one of its side-chain nitrogen atoms and the iron atom. Although arginine does not make a good ligand for transition metals, ligation of arginine to iron is not unprecedented, as it is observed in the structure of biotin synthase (60). Furthermore it is reported that in a hydrophobic environment a metal atom may be able to compete with an H⁺ ion for the nitrogen atoms of the arginine (61). In biotin synthase, the iron-bound arginine resides in a special surrounding, which is defined by a deep pocket in a triose phosphate isomerase barrel fold with a relatively large number of potential hydrogen-bonding partners (60). A similar environment can be identified around the side chain of Arg-75, where it sits deep inside the protein and has a potential to make H-bonds with Asp-99, His-111, Asp-131, and Met-133. EPR signals characteristic of the {Fe(NO)}⁷ (*S* = 3/2) complex were barely detectable in whole cells expressing the R75K and R75L proteins that were exposed to NO. Although ferrous iron could be reconstituted into the mutant proteins to a level similar to that observed with wild-type NorR, the EPR signal at *g* = 4.2, characteristic of the mononitrosyl complex, was not detectable *in vitro*. It therefore seems possible that these substitutions cause a defect in the interaction of the iron center with NO. The difference in the *in vivo* phenotypes of these mutants may arise from the lysine side chain, which, like arginine, may interact with Fe but lock it in an inactive state. If the iron atom in NorR is hexa-coordinated as predicted and ligand displacement is necessary to accommodate bound NO, then Arg-75 is a good candidate for such a role. It may not only relinquish a coordination site for NO, but it also has the potential to stabilize the NO interaction by hydrogen bonding.

Although the structural model we propose for the ferrous iron center in Fig. 7 is not definitive and other models are feasible, the coordination proposed is consistent with the spectral features of NorR and the properties of the mutant proteins.

Electronic absorption spectroscopy and EPR parameters of cobalt-substituted NorR suggest that the cobalt ion is 5- or 6-coordinate in a distorted octahedral symmetry in agreement with the geometry of the structural model. In the hexa-coordinate model shown in Fig. 7 we propose that Asp-96 provides a bidentate ligand to the iron. We favor this model because the Fe binding site appears to be solvent-inaccessible, and it is unlikely (but not impossible) that a water molecule provides the sixth ligand. We cannot, however, exclude the possibility that Asp-96 is a monodentate ligand and iron is present in a pentavalent geometry. From the five candidate ligands to the metal ion center that we have identified, Arg-75, Cys-113, and Asp-131 are predicted to be located in a relatively rigid part of the protein, whereas Asp-96 and Asp-99 are housed in random coil or loop. The NO-activated activated switch may be related to conformational changes in this relatively flexible part of the iron coordination site. Our site-directed mutagenesis studies suggest that the iron center in NorR is highly sensitive to the ligand environment, because substitutions in the same residue give rise to mutants locked in either the "on" or the "off" states. Hence the ferrous iron center is sensitively poised to receive the NO signal, leading to activation of NorR and consequent expression of the NorVW reductase necessary for NO detoxification.

Acknowledgment—We thank Myles Cheesman for valuable advice on EPR and MCD spectroscopy.

REFERENCES

1. Zhao, Y., Brandish, P. E., Ballou, D. P., and Marletta, M. A. (1999) *Proc. Natl. Acad. Sci. U. S. A.* **96**, 14753–14758
2. Boon, E. M., Huang, S. H., and Marletta, M. A. (2005) *Nat. Chem. Biol.* **1**, 53–59
3. Iyer, L. M., Anantharaman, V., and Aravind, L. (2003) *BMC Genomics* **4**, 5
4. Lee, Y. Y., Shearer, N., and Spiro, S. (2006) *Microbiology* **152**, 1461–1470
5. Nioche, P., Berka, V., Vipond, J., Minton, N., Tsai, A. L., and Raman, C. S. (2004) *Science* **306**, 1550–1553
6. Cruz-Ramos, H., Crack, J., Wu, G., Hughes, M. N., Scott, C., Thomson, A. J., Green, J., and Poole, R. K. (2002) *EMBO J.* **21**, 3235–3244
7. Ding, H. G., and Demple, B. (2000) *Proc. Natl. Acad. Sci. U. S. A.* **97**, 5146–5150
8. D'Autreaux, B., Touati, D., Bersch, B., Latour, J. M., and Michaud-Soret, I. (2002) *Proc. Natl. Acad. Sci. U. S. A.* **99**, 16619–16624
9. D'Autreaux, B., Tucker, N. P., Dixon, R., and Spiro, S. (2005) *Nature* **437**, 769–772
10. Spiro, S. (2007) *FEMS Microbiol. Rev.* **31**, 193–211
11. Bodenmiller, D. M., and Spiro, S. (2006) *J. Bacteriol.* **188**, 874–881
12. Filenko, N., Spiro, S., Browning, D. F., Squire, D., Overton, T. W., Cole, J., and Constantinidou, C. (2007) *J. Bacteriol.* **189**, 4410–4417
13. Nakano, M. M., Geng, H., Nakano, S., and Kobayashi, K. (2006) *J. Bacteriol.* **188**, 5878–5887
14. Rodionov, D. A., Dubchak, I. L., Arkin, A. P., Alm, E. J., and Gelfand, M. S. (2005) *PLoS Comput. Biol.* **1**, e5
15. Gardner, A. M., and Gardner, P. R. (2002) *J. Biol. Chem.* **277**, 8166–8171
16. Gardner, P. R., Gardner, A. M., Martin, L. A., and Salzman, A. L. (1998) *Proc. Natl. Acad. Sci. U. S. A.* **95**, 10378–10383
17. Hausladen, A., Gow, A., and Stamler, J. S. (2001) *Proc. Natl. Acad. Sci. U. S. A.* **98**, 10108–10112
18. Hausladen, A., Gow, A. J., and Stamler, J. S. (1998) *Proc. Natl. Acad. Sci. U. S. A.* **95**, 14100–14105
19. Gardner, A. M., Gessner, C. R., and Gardner, P. R. (2003) *J. Biol. Chem.* **278**, 10081–10086

20. Hutchings, M. I., Mandhana, N., and Spiro, S. (2002) *J. Bacteriol.* **184**, 4640–4643
21. Mukhopadhyay, P., Zheng, M., Bedzyk, L. A., LaRossa, R. A., and Storz, G. (2004) *Proc. Natl. Acad. Sci. U. S. A.* **101**, 745–750
22. Gardner, A. M., Helmick, R. A., and Gardner, P. R. (2002) *J. Biol. Chem.* **277**, 8172–8177
23. Vicente, J. B., and Teixeira, M. (2005) *J. Biol. Chem.* **280**, 34599–34608
24. Studholme, D. J., and Dixon, R. (2003) *J. Bacteriol.* **185**, 1757–1767
25. Ho, Y. S., Burden, L. M., and Hurley, J. H. (2000) *EMBO J.* **19**, 5288–5299
26. Aravind, L., and Ponting, C. P. (1997) *Trends Biochem. Sci.* **22**, 458–459
27. Zhang, X., Chaney, M., Wigneshweraraj, S. R., Schumacher, J., Bordes, P., Cannon, W., and Buck, M. (2002) *Mol. Microbiol.* **45**, 895–903
28. Ray, P., Smith, K. J., Parslow, R. A., Dixon, R., and Hyde, E. I. (2002) *Nucleic Acids Res.* **30**, 3972–3980
29. Tucker, N. P., D'Autreaux, B., Studholme, D. J., Spiro, S., and Dixon, R. (2004) *J. Bacteriol.* **186**, 6656–6660
30. Pohlmann, A., Cramm, R., Schmelz, K., and Friedrich, B. (2000) *Mol. Microbiol.* **38**, 626–638
31. Shingler, V. (1996) *Mol. Microbiol.* **19**, 409–416
32. Enemark, J. H., and Feltham, R. D. (1974) *Coord. Chem. Rev.* **13**, 339–406
33. Stookey, L. L. (1970) *Anal. Chem.* **42**, 779–781
34. Lin, J., and Kester, D. R. (1992) *Mar. Chem.* **38**, 283–301
35. Thompson, J. C., and Mottola, H. A. (1984) *Anal. Chem.* **56**, 755–757
36. Aasa, R., and Vänngård, T. (1975) *J. Magn. Reson.* **19**, 308–315
37. Arciero, D. M., Orville, A. M., and Lipscomb, J. D. (1985) *J. Biol. Chem.* **260**, 14035–14044
38. Ginalski, K., Elofsson, A., Fischer, D., and Rychlewski, L. (2003) *Bioinformatics* **19**, 1015–1018
39. Moore, L. J., and Kiley, P. J. (2001) *J. Biol. Chem.* **276**, 45744–45750
40. Solomon, E. I., Brunold, T. C., Davis, M. I., Kemsley, J. N., Lee, S. K., Lehnert, N., Neese, F., Skulan, A. J., Yang, Y. S., and Zhou, J. (2000) *Chem. Rev.* **100**, 235–350
41. Chauvin, A. S., Frapart, Y. M., Vaissermann, J., Donnadiou, B., Tuchagues, J. P., Chottard, J. C., and Li, Y. (2003) *Inorg. Chem.* **42**, 1895–1900
42. Clay, M. D., Emerson, J. P., Coulter, E. D., Kurtz, D. M., Jr., and Johnson, M. K. (2003) *J. Biol. Inorg. Chem.* **8**, 671–682
43. Yikilmaz, E., Xie, J., Brunold, T. C., and Miller, A. F. (2002) *J. Am. Chem. Soc.* **124**, 3482–3483
44. Fujisawa, H., and Hayaishi, O. (1968) *J. Biol. Chem.* **243**, 2673–2681
45. Davis, J. C., Lin, S. S., and Averill, B. A. (1981) *Biochemistry* **20**, 4062–4067
46. Martinelli, R. A., Hanson, G. R., Thompson, J. S., Holmquist, B., Pilbrow, J. R., Auld, D. S., and Vallee, B. L. (1989) *Biochemistry* **28**, 2251–2258
47. Bennett, B., and Holz, R. C. (1997) *Biochemistry* **36**, 9837–9846
48. Breece, R. M., Costello, A., Bennett, B., Sigdel, T. K., Matthews, M. L., Tierney, D. L., and Crowder, M. W. (2005) *J. Biol. Chem.* **280**, 11074–11081
49. Banci, L., Bencini, A., Benelli, C., Gatteschi, D., and Zanchini, C. (1982) in *Structure and Bonding. Vol. 52: Structures versus Special Properties*, pp. 37–86, Springer-Verlag, New York
50. Werth, M. T., Tang, S.-F., Formicka, G., Zeppezauer, M., and Johnson, M. K. (1995) *Inorg. Chem.* **34**, 218–228
51. Vasak, M., Kagi, J. H., Holmquist, B., and Vallee, B. L. (1981) *Biochemistry* **20**, 6659–6664
52. Griep, M. A., Adkins, B. J., Hromas, D., Johnson, S., and Miller, J. (1997) *Biochemistry* **36**, 544–553
53. Outten, C. E., Tobin, D. A., Penner-Hahn, J. E., and O'Halloran, T. V. (2001) *Biochemistry* **40**, 10417–10423
54. Clay, M. D., Jenney, F. E., Jr., Hagedoorn, P. L., George, G. N., Adams, M. W., and Johnson, M. K. (2002) *J. Am. Chem. Soc.* **124**, 788–805
55. Martinez, S. E., Wu, A. Y., Glavas, N. A., Tang, X. B., Turley, S., Hol, W. G., and Beavo, J. A. (2002) *Proc. Natl. Acad. Sci. U. S. A.* **99**, 13260–13265
56. Cramm, R., Busch, A., and Strube, K. (2006) *Biochem. Soc. Trans.* **34**, 182–184
57. Clay, M. D., Cosper, C. A., Jenney, F. E., Jr., Adams, M. W., and Johnson, M. K. (2003) *Proc. Natl. Acad. Sci. U. S. A.* **100**, 3796–3801
58. Busch, A., Strube, K., Friedrich, B., and Cramm, R. (2005) *Biochem. Soc. Trans.* **33**, 193–194
59. Klink, A., Elsner, B., Strube, K., and Cramm, R. (2007) *J. Bacteriol.* **189**, 2743–2749
60. Berkovitch, F., Nicolet, Y., Wan, J. T., Jarrett, J. T., and Drennan, C. L. (2004) *Science* **303**, 76–79
61. Fairlie, D. P., Jackson, W. G., Skelton, B. W., Wen, H., White, A. H., Wickramasinghe, W. A., Woon, T. C., and Taube, H. (1997) *Inorg. Chem.* **36**, 1020–1028

**Analysis of the Nitric Oxide-sensing Non-heme Iron Center in the NorR
Regulatory Protein**

Nicholas P. Tucker, Benoît D'Autréaux, Faridoon K. Yousafzai, Shirley A. Fairhurst,
Stephen Spiro and Ray Dixon

J. Biol. Chem. 2008, 283:908-918.

doi: 10.1074/jbc.M705850200 originally published online November 14, 2007

Access the most updated version of this article at doi: [10.1074/jbc.M705850200](https://doi.org/10.1074/jbc.M705850200)

Alerts:

- [When this article is cited](#)
- [When a correction for this article is posted](#)

[Click here](#) to choose from all of JBC's e-mail alerts

This article cites 60 references, 31 of which can be accessed free at
<http://www.jbc.org/content/283/2/908.full.html#ref-list-1>